ACS OMEGA

http://pubs.acs.org/journal/acsodf

Article

A Sandwich Metal−Insulation−Metal Composite for Magnetoelectric Memory: Experiment and Modeling

Jia-wei Zhang,* Usama Mahmood, Geng Fu, Fan Xu, Tianhao Li, and Yifan Liu

Cite This: *ACS Omega* 2021, 6, 35023−35029

Read Online

ACCESS | Metrics & More | Article Recommendations

ABSTRACT: Driven by the development of internet technology, higher requirements on information materials and data storage devices were demanded. To improve the work efficiency and performance of the new generation of information materials and data storage devices, the magnetoelectric (ME) coupling and storage mechanism of magnetoelectric composites deserve more attention. Here, we explored the influence of applied magnetic fields on the output voltage on a metal−insulation−metal (MIM) sandwich composite for realizing the magnetoelectric memory by experiments and modeling. It is found that the DC magnetic field (H_{dc}) and the output voltage of the polyvinylidene fluoride film are linearly correlated. At a frequency of 1 kHz, the magnetoelectric voltage coefficient is 60.71 mV cm^{-1} Oe^{-1}, which is evidently larger than that of other film materials. From this work, we can conclude that the MIM sandwich composite could generate higher magnetoelectric voltage under the AC magnetic field (H_{ac}) with higher frequency, which could be used as the magnetoelectric memory device, and provides significant support for improving the performance of magnetoelectric memory devices and the whole internet system.

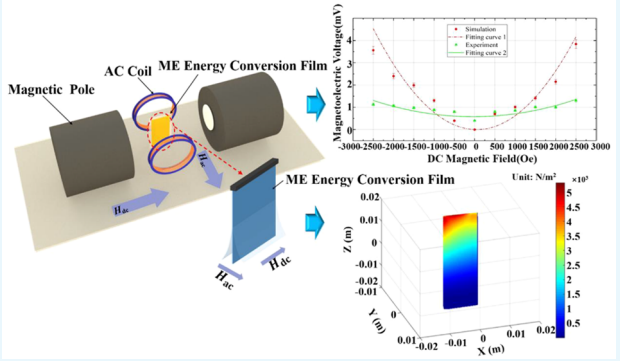

INTRODUCTION

The digital era urges for data memory devices with excellent performance,[1−3] which are widely used in internet communication, wearable biomedical devices, artificial intelligence, and so on.[4−9] Magnetoelectric memory controlled by the electric field has recently developed a lot of interest because of the low cost and high efficiency.[9−11] In order to develop new generation magnetoelectric memory, it is essential to further explore the simpler structures and magnetoelectric material with higher performance of magnetoelectric energy conversion.[10,12] At present, there are a lot of magnetoelectric experiments for exploring the magnetoelectric coupling and storage mechanism of magnetoelectric composites.

In 2017, Zong et al.[13] developed a novel cellulose-based magnetoelectric laminate structure. The maximum magnetoelectric coefficient of the novel structure was 1.41 V cm^{-1} Oe^{-1} under the applied H_{ac} and H_{dc}. However, the cellulose structure consisting of metglas−epoxy−gold electrode−cellulose film−gold electrode was relatively complicated. In 2020, Hyeon et al.[4] explored the performance of poly(vinylidene fluoride-co-trifluoroethylene) laminated onto a magnetostrictive multilayer metglas under the applied H_{ac} with constant frequency by experiments and finite element method (FEM). However, the relationship between H_{dc} and magnetoelectric performance of this structure was not explored. In 2021, Wu et al.[6] investigated the magnetoelectric effect of the mica substrate attached on both sides of flexible piezoelectric PZT films under the applied H_{ac} and H_{dc}. A more significant magnetoelectric coefficient could be observed. However, the modeling ignored in their work could help to evaluate the experimental results more intuitively and accurately.

Based on the above-mentioned investigations, this paper proposed the MIM structure, which comprised two sliver electrodes laminated on both sides of the polyvinylidene fluoride (PVDF) film. Its ME effect was explored in a different way from the coupling of magnetostrictive/piezoelectric phases. Compared to traditional ME composites with complex structures, the sandwich metal−insulation−metal (MIM) composite in this work presented a better trade-off between the conversion response and the flexibility. The MIM composite proposed in this work only consisted of two sliver electrodes sputtered on both sides of piezoelectric material, which was prone to achieve the ME coupling without requiring the magnetostrictive phase. Additionally, with low cost and high flexibility, the MIM composite was prone to be manufactured in various sizes or shapes. To verify the

Received: October 11, 2021
Accepted: November 23, 2021
Published: December 8, 2021

experiment's accuracy, the model was established to analyze the magnetoelectric property of the MIM composite. Moreover, the MIM composite was placed in the H_{dc} and H_{ac} with variable frequency to simulate the actual operating conditions. When the applied H_{ac} generated by the electric conducting coil penetrated the metal electrodes, eddy currents were generated on the metal electrodes by the Faraday effect. Ampere forces generated by the applied H_{dc} acted on the sandwich MIM composites, leading to the generation of ME voltage. The modeling and experimental data on the sandwich MIM composites with simple structure exhibited excellent magnetoelectric properties when exposed to the eddy current, H_{dc} and H_{ac}. The ME response and vibration in the PVDF film can be controlled by changing the magnetic field (AC and DC) and the eddy current, respectively. This experiment and modeling were divided into two sections. The first section explored the influence of the applied H_{dc} and H_{ac} on the output voltage of the sandwich MIM composite. Specifically, the H_{ac} (0 to 20 Oe) with a frequency of 1 kHz and the H_{dc} (−2500 to 2500 Oe) were applied on the sandwich MIM composite, respectively. The second section of this experiment was to investigate the influence of the frequency of the applied H_{ac} on the output voltage of the MIM composite. When the H_{dc} and H_{ac} were set to 1000 and 5 Oe, respectively, and the frequency of H_{ac} changed from 10 to 1000 Hz, the output voltage of the sandwich MIM composite was measured and investigated. The investigation on ME effect of the sandwich MIM composite provided significant support and reference for developing excellent magnetoelectric memory devices.

RESULTS AND DISCUSSION

Magnetoelectric Responses of the Sandwich MIM Composite. The vibration/deformation in the PVDF material results from the eddy current induced by the increase of H_{ac}. When the vibration intensifies, the output voltage generated in the sandwich MIM composite also increases. Three cases are studied to analyze the corresponding vibration and output voltage generated in the sandwich MIM composite. Figure 1 shows the increase in voltage on the sandwich ME composite, attributed to the vibration caused by applying AC magnetic field (from 0 to +20 Oe) and without H_{dc}. The measurement indicates that the silver layer on the sample generates an eddy current under the H_{ac} and without H_{dc}, which could generate

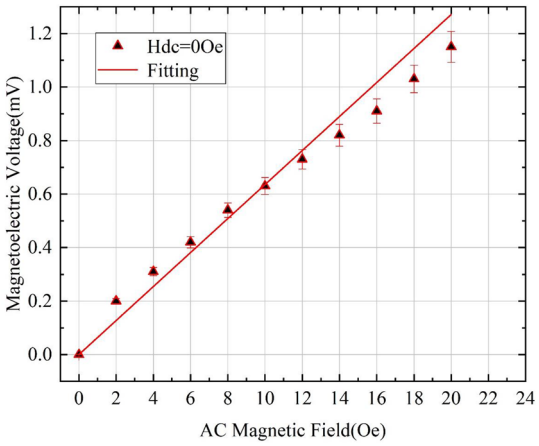

Figure 1. Linear relationship between ME voltage and AC magnetic field (@f = 1 kHz).

the thermoelectric effect. Since PVDF is a kind of piezoelectric and thermoelectric material, a thermoelectric effect generates voltage at a certain heat.[14] The H_{ac} dependence of the ME voltage signal exhibits that ME voltage is only induced by the thermoelectric effect instead of ME effect. Under the applied H_{dc}, the induced magnetoelectric effect and the thermoelectric effect are distinguished by comparing the magnitude of the voltage generated by the thermoelectric effect. Compared with the magnetoelectric voltage under the condition of merging H_{dc} with H_{ac}, the ME voltage without the applied H_{ac} is so low that it may be negligible.

Figure 2 shows the increase in ME voltage on the sandwich MIM composite due to the vibration generated by applying H_{ac}

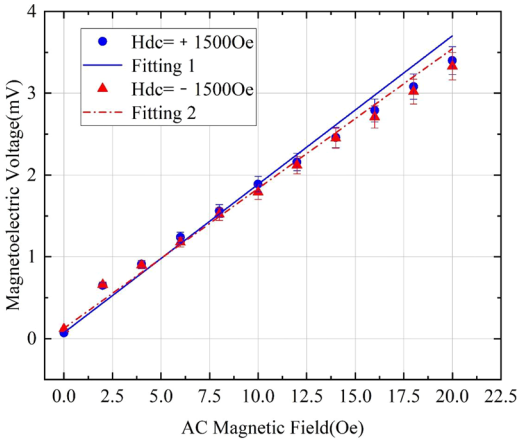

Figure 2. Amplitude of ME voltage as a function of AC magnetic field amplitude for different DC magnetic fields (@f = 1 kHz).

from 0 to 20 Oe with a frequency of 1 kHz and H_{dc} from −1500 to 1500 Oe. As shown in Figure 3, a quadratic-type

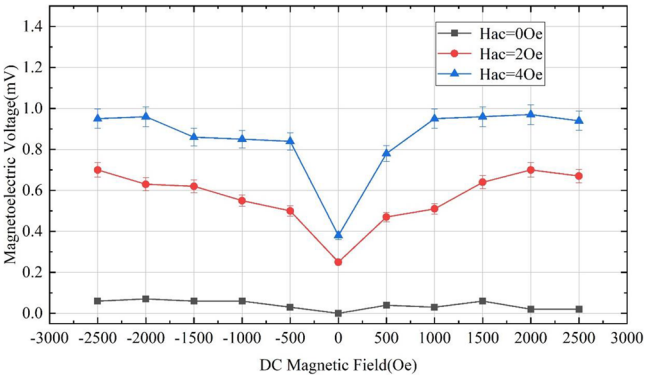

Figure 3. Amplitude of ME voltage as a function of DC magnetic field.

magnetoelectric response generates on the sandwich MIM composite under an H_{ac} value of 2, 4 Oe with a frequency of 1 kHz when the H_{dc} is varied from −2500 Oe to 2500 Oe. In addition, when the H_{ac} is zero, the ME voltage of the sandwich MIM composite remains at around zero, because the eddy current is not generated without H_{ac}. Based on the above results, we can find the ME output voltage has a strong dependence of H_{dc}. Therefore, the amplitude of a DC magnetic field can be obtained by measuring the ME output voltage under a specific H_{ac}.

https://doi.org/10.1021/acsomega.1c05678
ACS Omega 2021, 6, 35023−35029

Influence of DC Magnetic Field on PVDF Samples. Figure 4 shows the simulation and experimental results of the

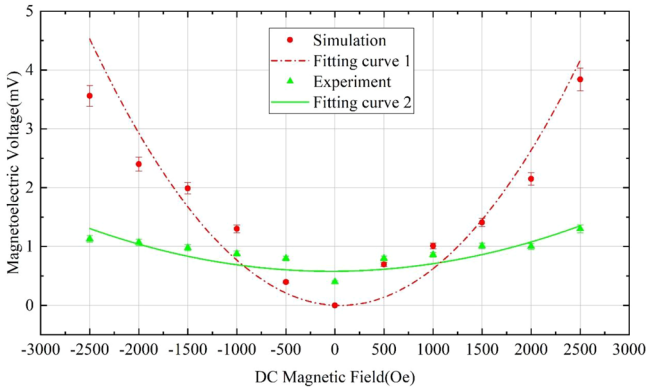

Figure 4. Comparison of ME effect between the simulation and experiment (@f= 1 kHz; H_{ac} =5 Oe).

magnetoelectric voltage under H_{dc} from −2500 to 2500 Oe. The results show that the magnetoelectric voltage is proportional to the applied H_{dc}, which could be attributed to the increase of the Lorenz force and bending degree on the sandwich MIM composite. When the H_{dc} is zero, the ME output voltage reaches the minimum value. The reason for the minimum ME output voltage is that there has not the Lorenz force when the H_{dc} is zero. In addition, there is a deviation of the minimum ME output voltage between the experimental measurement and simulation result, which can be attributed to the thermoelectric effect. As shown in Figure 4, the above mentioned results are consistent with the experimental result shown in Figure 1, which further confirms the thermoelectric effect. The thermoelectric effect is caused by the generation of eddy current in the metal layer on the sample under the H_{ac} and without H_{dc}. Then, a deviation between the simulation and experimental results is obtained when moving the vortex center along the sample length direction.[15]

Influence of the Frequency of AC Magnetic Field on the Output Voltage of PVDF Samples. Figure 5 shows experimental results of magnetoelectric voltage with the

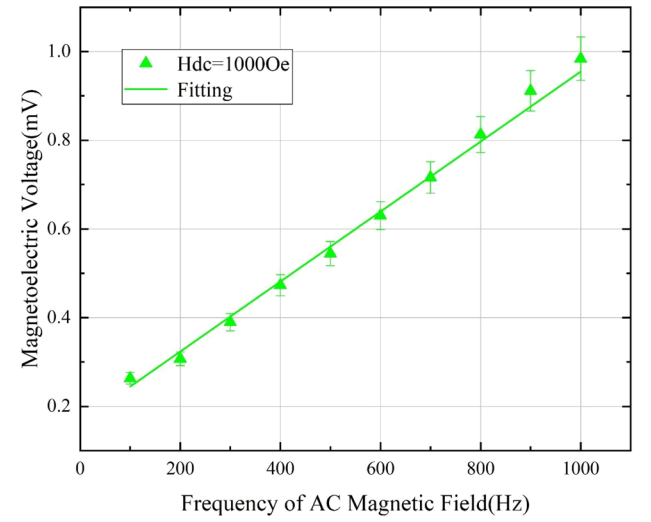

Figure 5. Frequency dependence of the ME voltage signal (@H_{ac} = 5 Oe, H_{dc} = 1000 Oe).

frequency of H_{ac} from 10 to 1000 Hz. The results show that with the increase of the frequency of the H_{ac}, the larger induced current and output voltage on the sandwich MIM composite can be observed, which results from the increase of magnetic field strength through the sandwich MIM composite. With the increase of AC magnetic field frequency, the stronger the magnetic field passing through the silver metal surface, the larger induced current and the larger the output voltage of the ME film can be generated. Due to the influence of frequency fluctuations, the output voltage fluctuates upward. The output voltage increases quickly with the increase of the frequency within 1 kHz. In addition, the behavior of applied H_{ac} and H_{dc} and the influence of the frequency of the applied H_{ac} on the output voltage are quite similar as they show linear responses to the output voltage. In this case, the ME effects are evidently related to the AC magnetic field frequency. The frequency of H_{ac} dependence of direct ME coefficients is relevant to the relative dielectric constant and the variation in the piezoelectric phase coupled with a magnetic field. The experiment results in Figure 5 show the linear response between the ME voltage and the frequency of between the ME voltage and the frequency of H_{ac}, which prove that the ME output voltage can be controlled by AC magnetic field frequency.

Mechanical Analysis of the ME Film under Lorentz Force. The equation of the electromagnetic properties of two-way combined matter is the basis for solving the problem of the magnetic field. Static magnetic field refers to the constant magnetic field generated by direct current. According to the theory of vector analysis, magnetic induction intensity is expressed as the spin of another vector. Under the applied AC and DC magnetic fields, the coupling between the Lorentz force produced by the metal electrode and the piezoelectric effect of the sample is used to achieve magnetoelectric conversion. When the applied H_{dc} penetrates the surface of the metal electrodes, a magnetic flux ϕ_{ac} is expressed as

$$\phi_{ac} = \iint_s \mu_0 h_{ac} dS \tag{1}$$

where S represents the surface area of the silver electrode; μ_0 is the magnetic permeability. According to Faraday's law of electromagnetic induction, induced currents are generated by AC magnetic field. The AC magnetic field h_{ac} is expressed as

$$h_{ac} = H_{ac} e^{j\omega t} \tag{2}$$

where ω= $2\pi f$ is the angular frequency, f = 1 kHz magnetic field frequency, and H_{ac} is the amplitude of the AC magnetic field. The electromotive force (E_f) in the metal electrode is expressed as[16]

$$E_f = -\frac{d\phi_{ac}}{dt} = -j\omega\mu_0 S H_{ac} e^{j\omega t} = -j\omega\mu_0 S h_{ac} = -j\omega\phi_{loop} \tag{3}$$

where ϕ_{loop} is the magnetic flux in the metal electrode.

Determining the current density of the eddy current is the key problem to explore the magnetoelectric coupling further. The eddy current is calculated using the current density J form of Ohm's law,

$$J = \sigma E \tag{4}$$

where σ is the conductivity of silver and E is the electric field induced by the alternating magnetic field. However, the relationship between E_f and E is expressed as

https://doi.org/10.1021/acsomega.1c05678
ACS Omega 2021, 6, 35023−35029

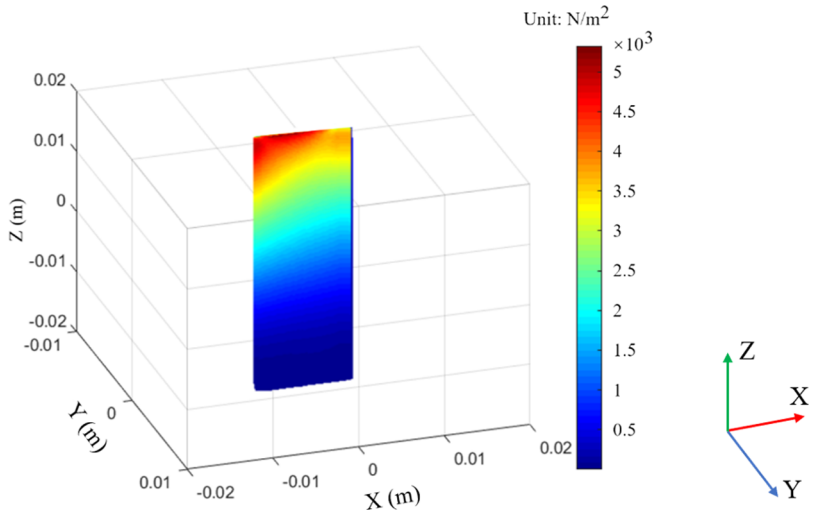

Figure 6. Simulation of the displacement diagram of ME beam.

Table 1. Comparison between ME Voltage Coefficients of Different Materials

types	materials	α (mV cm^{-1} Oe^{-1})
single-phase samples	Cr_2O_3 crystal @1 kHz[20]	20
particulate composite samples	P(VDF-TrFE) +0.3wt %Fe_3O_4 @5 kHz[21]	2.23
	P(VDF-TrFE) +72wt %$CoFe_2O_4$ @ 5 kHz[22]	40
multilayer samples	PZT/Alumina @ 4.9kHz[15]	79
	silver/PVDF/silver @1 kHz [this work]	60.71

$$E_f = \oint_L E\mathrm{d}L = -j\omega\mu_0 S H_{ac} e^{j\omega t} \tag{5}$$

where L is the circumference of the eddy current loop. Then, substituting eq 4 into eq 5, the eddy currents of the silver electrode can be expressed as

$$i_{edd} = \oint_L J\mathrm{d}L = -j\omega\mu_0\sigma S\pi(L/2)^2 H_{ac} e^{j\omega t} \tag{6}$$

when DC bias magnetic field acts on metal electrodes, a differential equation of Ampere force (d_F) expressed as eq 7[17] is generated in each current loop.

$$d_F = i_{edd}(dL \times B) = i_{edd}[dL \times (H_{dc} + H_{ac})] \tag{7}$$

where B is the magnetic induction vector, dL is a vector element of the loop's closed contour, and H_{dc} is the uniform applied magnetic field. Then, a moment subjected to each loop is expressed as

$$M = z \times F = i_{edd} m \times B = \mu_0 i_{edd}[m \times (H_{dc} + H_{ac})] \tag{8}$$

where z is the molecular magnetic moment of the eddy current loop and m is the area of the loop.

Finally, electrodes on both sides of the PVDF film are subjected to torques M_1 and M_2 because the sample is isotropic in the plane. Therefore, the torque of the PVDF film can be expressed as

$$M_{TOT} = 2M \tag{9}$$

However, the electromechanical modeling of the unimorph bender could be calculated based on eq 10.

$$\begin{cases} s_3 = S_{33}^D T_3 + g_{33} D_3 \\ E_3 = -g_{33} T_3 + \beta_{33}^T D_3 \end{cases} \tag{10}$$

where s_3, E_3, T_3, and D_3 are the strain, the electric field, the stress, and the electric displacement; g_{33} represents the piezoelectric constant; β_{33}^T and S_{33}^D express absolute permittivity and suppleness of the material, respectively.

Substituting the short circuit condition T_3= 0 in eq 10 yields

$$E_3 = dT_3 \tag{11}$$

Thus, the theoretical expression of the ME current I_{ME} induced by the Lorenz force is given by[18]

$$|I_{ME}| = \frac{\partial M_{TOT}}{\partial t} = 2j\omega\mu_0^2\sigma S^2 H_{dc} h_{ac} \tag{12}$$

In previous studies, only the free end of the bimorph is subjected to an external moment. The change of the generated electric charge can be expressed as[19]

$$Q = \frac{3d_{31}l}{t^2} M_{TOT} = \frac{-j6d_{31}l\omega\sigma\mu_0 S^2 H_{dc} h_{ac}}{t^2} \tag{13}$$

where d_{31}, t, and l are the transverse piezoelectric coefficient, the sample's thickness, and length, respectively. The magneto-electric voltage generated by Ampere forces can be expressed as

$$|V_{ME}| = \frac{Q}{C_z} = \frac{j6d_{31}l\omega\sigma\mu_0^2 S^2 H_{dc} h_{ac}}{t^2 C_z} \tag{14}$$

where C_z is the capacitance of the PVDF film.

Finally, the ME voltage coefficient α is calculated by solving eq 15.

$$\alpha = \frac{\mathrm{d}V_{ME}}{t \cdot \mathrm{d}H_{dc}} \tag{15}$$

https://doi.org/10.1021/acsomega.1c05678
ACS Omega 2021, 6, 35023−35029

As can be seen from Figure 6, when the applied H_{dc} is ±2500 Oe, the ME voltage coefficient reaches α = 60.71 mV cm^{-1} Oe^{-1} @1 kHz. As shown in Table 1, the optimal values of the ME voltage coefficient α are listed.

The model is built by the FEM. When the body load of the Lorenz force is loaded into the sandwich MIM composite, the total displacement of the ME film along the direction of thickness is shown in Figure 6. From this figure, when the Lorenz force is applied to the sandwich MIM composite, the sample is subjected to different torsional moments, which induces strain on the piezoelectric phase causing asymmetrical stress. The ME composite moves along the direction of thickness (Y) under the Lorenz force generated by the vortex current, which is consistent with the theoretical analysis. At the same time, as the DC magnetic field increases, the Lorentz force is also increased. The increase of Lorentz force leads to the increase of strain of the film, which further leads to the increase of the magnetoelectric voltage.

When the Lorentz force acts on the piezoelectric phase, the force and deformation are induced in the sample. As shown in Figure 7, its vibration direction is along the thickness direction

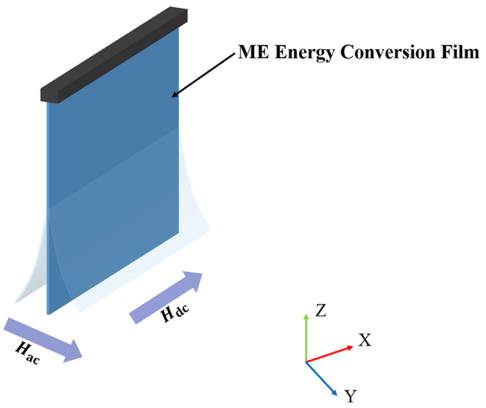

Figure 7. Schematic of the vibration mode of the ME film under AC and DC magnetic fields.

(Y) of the sample. Due to the piezoelectric effect, the surface charges of the sandwich ME composite migrate, and surface charges with opposite polarity are induced on two opposite surfaces. In this case, the PVDF layer of the tested material exhibits the magnetoelectric effect as piezoelectric ceramics.

From the previous analysis, it can be seen that under the Lorentz force generated by the eddy current, the sandwich MIM composite bends along the thickness direction. The surface of the sandwich MIM composite charges under the piezoelectric effect. A terminal into the electrostatic node is added to obtain the output potential on the sandwich MIM composite surface. Figure 8 reflects that a uniform surface potential distribution of the sandwich MIM composite under the condition of an AC magnetic field strength of 15 Oe with a frequency of 1 kHz.

As shown in Figure 9, with evident direct ME effect resembling the bulk ME composite, the flexible ME composite could be used in magnetoelectric memories, microdevice sensors, magnetic memories, oscillators, phase shifters, and the like. For the ME memories, the sensitivity is a significant issue. Specifically, when the ME sensitivity is around 1 μV Oe^{-1}, the response signal on the ME films could reach 100 μV under the media field up to 100 Oe. Consequently, the ME memories with larger ME coefficients could reach higher output signal at

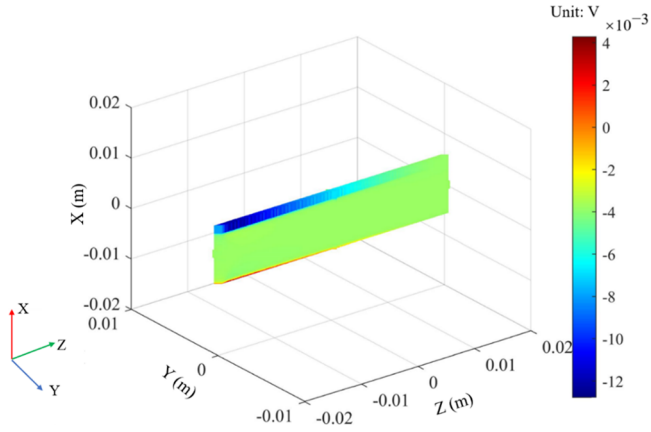

Figure 8. Simulation results of output voltage of the ME film.

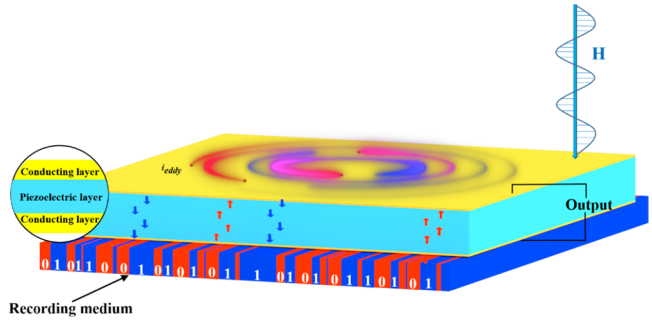

Figure 9. Schematic diagram of magnetoelectric memory.

a relatively weak magnetic field.[23] Based on the above description, the sandwich MIM composite has considerable potential in ME memory devices depending on the higher ME coefficient.

CONCLUSIONS

In conclusion, we fabricated a sandwich MIM composite which could be used for magnetoelectric memory devices. The sandwich MIM composite has higher ME voltage coefficients of 60.71 mV cm^{-1} Oe^{-1}, which is beneficial for the magnetoelectric conversion. Specifically, the ME output voltage increases with the increase of the applied DC magnetic field. In addition, when the H_{ac} is constant, the ME output voltage increases with the increase of H_{dc}. Moreover, the relationship between the frequency of H_{ac} and the ME output voltage exhibits a linear tendency. Finally, the simulation results are consistent with the experimental results, which reflects the model established in this paper could help to evaluate the experimental results more intuitively and accurately. It can be concluded that the sandwich MIM composite has considerable potential in magnetoelectric memory devices. This paper provides significant support for developing magnetoelectric memory devices, which is essential to develop the whole internet system and its subsystem in the future.

EXPERIMENT SECTION

Magnetoelectric Experiment. The sandwich MIM composite samples (40 × 10 × 0.028 mm) were subjected to the H_{ac} and H_{dc}, which were generated by two DC sources and one AC coil source. Firstly, the top of the sandwich MIM composite was vertically fixed on a specimen holder. Then, the

https://doi.org/10.1021/acsomega.1c05678
ACS Omega 2021, 6, 35023−35029

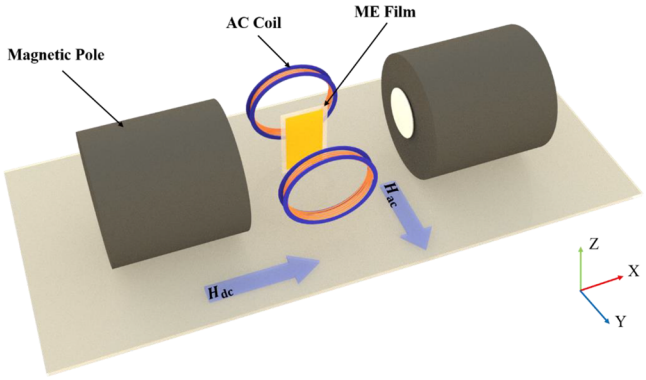

Figure 10. Schematic diagram of the experimental setup for the magnetoelectric measurement.

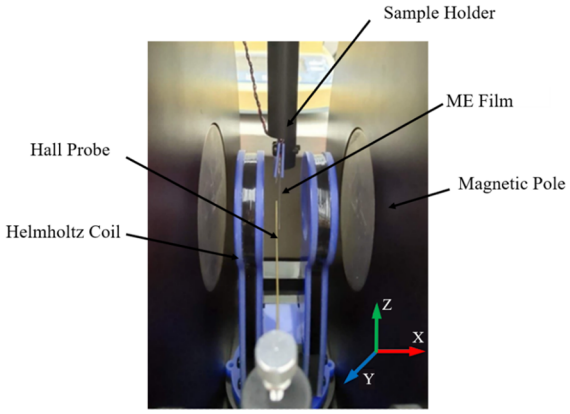

Figure 11. Enlarged image of the sample in the magnetic fields.

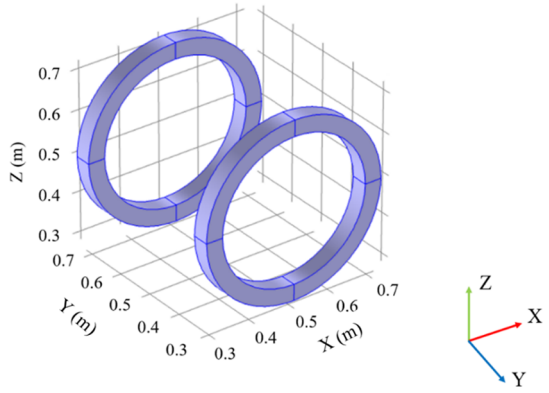

Figure 12. FEM simulation of the Helmholtz coil.

DC bias magnetic field driven by a DC programmable power current source (CH-Hall, F2030) was applied on both sides of the sample to ensure the sample's plane and DC magnetic field in the same direction. Two Helmholtz coils were driven by a voltage amplifier (NJFNKJ, HEAS-50) regulated by a waveform generator (RIGOL, DG1022U), while the AC magnetic field superimposed on a constant DC magnetic field was applied perpendicularly to the plane of the films, as shown in Figures 10 and 11. The magnitude of the magnetic field was measured with a tesla meter (CH-Hall, 1500). Finally, data acquisition equipment (CH-Hall, NET) was employed to store the measurement.

In this experiment, for the sandwich MIM composite, DC and AC magnetic fields were perpendicular to each other. The

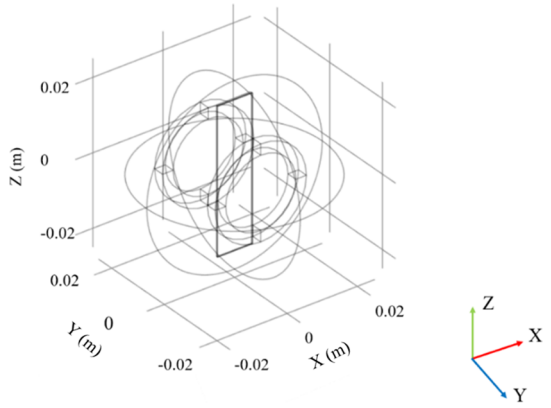

Figure 13. Modeling process of the ME film.

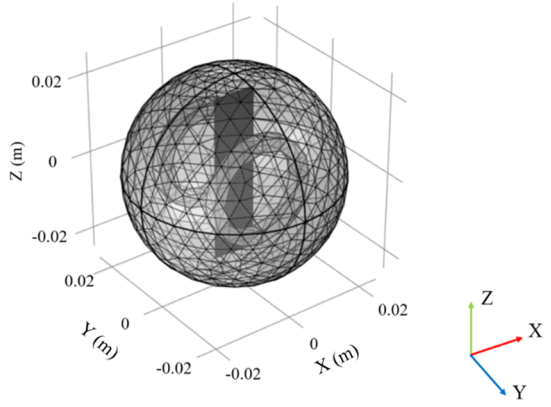

Figure 14. The mesh generation of the ME film.

induced Lorentz force was perpendicular to the sandwich MIM composite. This force vibrated the sandwich MIM composite, which led to the generation of the voltage in the sandwich MIM composite. Moreover, the magnetic flux induced by the eddy current penetrated into the silver electrode can be observed in the sandwich MIM composite. Because of the influence of DC bias magnetic field, the magnetoelectric output voltage and the vibration amplitude can be accurately regulated by manipulating the applied H_{ac} and H_{dc}.

Magnetoelectric Modeling. There were four interfaces considered in the simulation including magnetic fields interface, magnetic fields−solid interface, solid interface and electrostatic interface. The magnetic fields interface was mainly used to calculate the distribution of induced current and the surrounding magnetic field within the coil, conductor, and magnet. The magnetic fields−solid interface was defined by Ampere law. The solid interface was employed for calculating the displacements, stresses and strains of the ME film. The electrostatic interface was employed for calculating electric displacement field and potential distributions of ME film. The boundary condition, including the size of sample, magnetic flux vector and tangential components of the magnetic field etc., had been added.

The Helmholtz coils paralleled to each other can produce an alternating magnetic field, and the distance between the coils was equal to the radius of the coil, as shown in Figure 12. The simulated Helmholtz coil required adding coil nodes under the magnetic field interface and a current excitation of 0.5 kA in the coil.

https://doi.org/10.1021/acsomega.1c05678
ACS Omega 2021, 6, 35023−35029

According to the Figure 13, a magnetic field environment was simulated. The ME sample was placed in the alternating magnetic field space. The modeling space was cut into by the "finite element" area. The continuous solution domain was separated into a limited number of subregions to solve the physical variables of each subregion, and each subregion was continuous and coordinated, which was beneficial for improving the computational accuracy and computional sensitivity. Figure 14 showed the mesh generation of the ME film.

AUTHOR INFORMATION

Corresponding Author

Jia-wei Zhang − *School of Electrical Engineering, Xi'an University of Technology, Xi'an 710048, China;* orcid.org/0000-0002-2947-0124; Email: jwzhang@xaut.edu.cn

Authors

Usama Mahmood − *School of Electrical Engineering, Xi'an University of Technology, Xi'an 710048, China*

Geng Fu − *School of Electrical Engineering, Xi'an University of Technology, Xi'an 710048, China*

Fan Xu − *School of Electrical Engineering, Xi'an University of Technology, Xi'an 710048, China*

Tianhao Li − *Chengde State Grid Corporation of China, Chengde 067000, China*

Yifan Liu − *School of Electrical Engineering, Xi'an Jiaotong University, Xi'an 710049, China*

Complete contact information is available at: https://pubs.acs.org/10.1021/acsomega.1c05678

Notes

The authors declare no competing financial interest.

ACKNOWLEDGMENTS

This work was supported by the National Natural Science Foundation of China (NSFC) (Grant No. 51877031 and Grant No. 62061136009) and the High-level Talents Plan of Shaanxi Province.

REFERENCES

(1) Mishra, S.; Das, A.; Akhtar, A. J. Room temperature tuning of non volatile magnetoelectric memory in Al doped $Sr_3Co_2Fe_{24}O_{41}$. *Ceram. Int.* **2021**, *47*, 29261−29266.

(2) Zhang, B.; Fan, F.; Xue, W.; Liu, G.; Fu, Y.; Zhuang, X.; Xu, X.; Gu, J.; Li, R.; Chen, Y. Redox gated polymer memristive processing memory unit. *Nat. Commun.* **2019**, *10*, 736.

(3) Gao, S.; Yi, X.; Shang, J.; Liu, G.; Li, R. Organic and hybrid resistive switching materials and device. *Chem. Soc. Rev.* **2019**, *48*, 1531−1565.

(4) Hyeon, D. Y.; Nam, C.; Ham, S. S.; Hwang, G. T.; Yi, S.; Kim, K. T.; Park, K. Enhanced Energy Conversion Performance of a Magneto−Mechano−Electric Generator Using a Laminate Composite Made of Piezoelectric Polymer and Metallic Glass. *Adv. Electron. Mater.* **2021**, *7*, No. 2000969.

(5) Zahoor, F.; Azni Zulkifli, T. Z.; Khanday, A. Resistive Random Acess Memory (RRAM): an overview of materials, switching mechanism, performance, multilevel cell (mlc) storage, modeling and applications. *Nanoscale Res. Lett.* **2020**, *15*, 1−26.

(6) Yang, N.; Wu, H.; Wang, S.; Yuan, L.; Zhang, J.; Sokolov, O.; Bichurin, M. I.; Wang, L.; Wang, Y. Ultrasensitive flexible magnetoelectric sensor. *APL Mater.* **2021**, *9*, No. 021123.

(7) Chang, L.; Li, C. L.; Zhang, Z.; Xiao, J.; Liu, Q.; Zhu, Z.; Li, W.; Zhu, Z.; Yang, S.; Zhou, J. Energy-efficient computing-in-memory architecture for AI processor: device, circuit, architecture perspective. *Sci. China Inf. Sci.* **2021**, *64*, 160403.

(8) Yuan, Z.; Liu, J.; Li, X.; Yan, L.; Chen, H.; Wu, B.; Yang, Y.; Sun, G. NAS4RRAM: neural network architecture search for inference on RRAM-based accelerators. *Sci. China Inf. Sci.* **2021**, *64*, 160407.

(9) Shen, J.; Cong, J.; Shang, D.; Chai, S.; Shen, S.; Zhai, K.; Sun, Y. A multilevel nonvolatile magnetoelectric memory. *Sci. Rep.* **2016**, *6*, 34473.

(10) Han, Y.; Zhang, Z.; Wang, F.; Mi, W.; Zhang, K. Fabrication and characterization of a magnetoelectric memory cell of $50Ba(Zr_{0.2}Ti_{0.8})O_3-50Ba_{0.7}Ca_{0.3}TiO_3/Fe_{70}Ga_{30}$. *Mater. Lett.* **2016**, *170*, 192−195.

(11) Zhou, Z.; Zhao, S.; Gao, Y.; Wang, X.; Nan, T.; Sun, N. X.; Yang, X.; Liu, M. The memory effect of magnetoelectric coupling in FeGaB/NiTi/PMN-PT multiferroic heterostructure. *Sci. Rep.* **2016**, *6*, 20450.

(12) Bur, A.; Wong, K.; Zhao, P.; Lynch, C. S.; Amiri, P. K.; Wang, K. L.; Carman, G. P. Electrical control of reversible and permanent magnetization reorientation for magnetoelectric memory devices. *Appl. Phys. Lett.* **2011**, *98*, 262504.

(13) Zong, Y.; Zheng, T.; Martins, P.; Lanceros-Mendez, S.; Yue, Z.; Higgins, M. J. Cellulose-based magnetoelectric composites. *Nat. Commun.* **2017**, *8*, 38.

(14) Hu, S.; Zeng, S.; Li, X.; Jiang, J.; Yang, W.; Chen, Y.; Li, M.; Zheng, J. Flexible and high performance of n-type thermoelectric PVDF composite film induced by nickel nanowires. *Mater. Des.* **2020**, *188*, No. 108496.

(15) Huong Giang, D. T.; Tam, H. A.; Ngoc Khanh, V. T.; Vinh, N. T.; Anh Tuan, P.; van Tuan, N.; Thi Ngoc, N.; Duc, N. H. Magnetoelectric Vortex Magnetic Field Sensors Based on the Metglas/PZT Laminates. *Sensors* **2020**, *20*, 2810.

(16) Zhang, J. W.; Belouadah, R.; Lebrun, L.; Guyomar, D. Magnetoelectric Phenomena of Insulator Polymers after Corona Poling: Procedure and Experiments. *Sens. Actuators A Phys.* **2014**, *220*, 112−117.

(17) Guiffard, B.; Guyomar, D.; Garbuio, L.; Belouadah, R.; Zhang, J.; Cottinet, P. J. Eddy current induced magnetoelectricity in a piezoelectric unimorph bender. *Appl. Phys. Lett.* **2010**, *96*, No. 044105.

(18) Le, M. Q.; Belhora, F.; Cornogolub, A.; Cottinet, P. J.; Lebrun, L.; Hajjaji, A. Enhanced magnetoelectric effect for flexible current sensor applications. *J. Appl. Phys.* **2014**, *115*, 194103−194103.

(19) Wang, Q.; du, X. H.; Xu, B.; Cross, L. E. Theoretical analysis of the sensor effect of cantilever piezoelectric benders. *J. Appl. Phys.* **1999**, *85*, 1702−1712.

(20) Guyomar, D.; Guiffard, B.; Belouadah, R.; Petit, L. Two-phase magnetoelectric nanopowder/polyurethane composites. *J. Appl. Phys.* **2008**, *104*, No. 074902.

(21) Belouadah, R.; Seveyrat, L.; Guyomar, D.; Guiffard, B.; Belhora, F. Magnetoelectric coupling in Fe_3O_4/P(VDF-TrFE) nanocomposites. *Sens. Actuators A Phys.* **2016**, *247*, 298−306.

(22) Martins, P.; Gonçalves, R.; Lanceros-Mendez, S.; Lasheras, A.; Gutiérrez, J.; Barandiarán, J. M. Effect of filler dispersion and dispersion method on the piezoelectric and magnetoelectric response of CoFe2O4/P(VDF-TrFE) nanocomposites. *Appl. Surf. Sci.* **2014**, *313*, 215−219.

(23) Ma, J.; Hu, J. M.; Li, Z.; Nan, C. W. Recent Progress in Multiferroic Magnetoelectric Composites: from Bulk to Thin Films. *Adv. Mater.* **2011**, *23*, 1062−1087.